ARTICLE

Revisiting dithiadiaza macrocyclic chelators for copper-64 PET imaging

Received 00th January 20xx,
Accepted 00th January 20xx

DOI: 10.1039/x0xx00000x

Sergey Shuvaev,*[a] Elizaveta Suturina,[b] Nicholas J. Rotile,[a] Andrei Astashkin,[c] Christopher J. Ziegler,[d] Alana W. Ross,[a] Tia Walker,[e] Peter Caravan[a] and Ian Taschner*[e]

Synthesis and characterisation of a dithiadiaza chelator **NSNS2A**, as well as copper complexes thereof are reported in this paper. Molecular structures of copper (I/II) complexes were calculated using density-functional theory (DFT) further validated by both NMR and EPR spectroscopy. DFT calculations revealed a switch in the orientation of tetragonal distortion upon protonation, which might be responsible for poor stability of **$Cu^{(II)}$NSNS2A** complex in aqueous media, whilst the same switch in tetragonal distortion was experimentally observed by changing the solvent. The chelator was radiolabeled with ^{64}Cu and evaluated using PET/MRI in rats. Despite a favorable redox potential to stabilize the cuprous state in vivo, **$^{64}Cu^{(II)}$NSNS2A** complex showed suboptimal stability compared to its tetraazamacrocyclic analogue, **^{64}Cu(TE2A)**, with a significant ^{64}Cu uptake in the liver.

Introduction

Copper homeostasis in the body remains a subject of an active debate, given its essential role in various biological processes. Many of these processes involve reversible switching between Cu(I) and Cu(II), suggesting an intrinsic capacity of biological systems to stabilize both cupric and cuprous states.[1] Endogenous copper complexes may experience similar redox transformations, which affect their *in vivo* stability but often escape the scrutiny when designing new radiopharmaceuticals, including ^{64}Cu PET tracers. Although very high kinetic inertness and thermodynamic stability was reported for macrocyclic chelators widely used for binding ^{64}Cu *in vitro*, the residual uptake by the hepatobiliary system was reported in preclinical studies.[2] If chemically intact in the body, these hydrophilic chelates would experience an exclusively renal clearance, thereby the residual uptake in the liver suggests a possible transchelation mediated by liver proteins, as was later confirmed by size-exclusion radio-HPLC.[3] Substantial progress has been achieved by rigidifying ligand structures to further enhance the stability of their Cu(II) complexes *in vitro*, giving rise to a cross-bridged CB-TE2A chelator, as well as hexaazamacrobicyclic cage-like sarcophagine family.[4] Their use resulted in an increased stability of ^{64}Cu tracers against transchelation *in vivo*. Although CB-TE2A required harsher radiolabelling conditions, often incompatible with the use of conjugated biological vectors, sarcophagine chelators combined a very high kinetic inertness *in vivo* with mild radiolabelling conditions, resulting in their rising popularity in preclinical studies.[5, 6]

Notwithstanding the fact that the lability of Cu(I) species formed by reduction of the Cu(II) complexes was suggested among possible culprits behind the observed *in vivo* transchelation in complexes with some tetraazamacrocycles,[7] only few recent attempts have been made to design ligands that can support both cuprous and cupric states.[8-10] For example, the transchelation of copper to intracellular proteins upon reduction to Cu(I) has been suggested as the rationale behind the observed signal enhancement in patients with hypoxic tumours, who were administered with a cell-permeable tracer ^{64}Cu-ATSM.[11] Meanwhile, most extracellular chelators have been designed to provide an increased redox stability of the Cu(II) state by decreasing the $E_{1/2}$ potential to prevent a possible *in vivo* reduction in the first place.[7, 12]

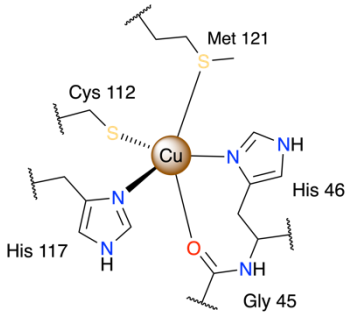

Figure 1. Coordination environment of the Type 1 copper binding site in azurin.

[a] *A. A. Martinos Center for Biomedical Imaging and the Institute for Innovation in Imaging, Massachusetts General Hospital, Harvard Medical School, Charlestown, MA 02129, USA. E-mail: sshuvaev@mgh.harvard.edu*
[b] *Department of Chemistry, University of Bath, Claverton Down, Bath BA2 7AY, UK. E-mail: e.suturina@bath.ac.uk*
[c] *Department of Chemistry and Biochemistry, University of Arizona, Tucson, AZ 85721, USA.*
[d] *Department of Chemistry, University of Akron, Akron, OH 44325, USA*
[e] *Department of Chemistry, Indiana University Northwest, Gary, IN 46408, USA. E-mail: itaschne@iun.edu*
† Footnotes relating to the title and/or authors should appear here.
Electronic Supplementary Information (ESI) available: [details of any supplementary information available should be included here]. See DOI: 10.1039/x0xx00000x

Unlike oxophilic cupric ions, larger cuprous ions are known to preferentially form stable tetrahedral complexes with softer donors, such as thiols and thioethers. In biological systems, active sites of cuproenzymes usually share either a tetrahedral N_2S_2 or five-coordinate N_2S_2O coordination motifs of copper ions that can reversibly switch between Cu(I) and Cu(II) states.[13] For instance, the five-coordinate copper ion in Type 1 copper site in a bacterial blue copper protein azurin is coordinated by two histidine N and one cysteine S atoms in an equatorial plane, as well as by axially bound amide oxygen of glycine and a thioether of methionine (Fig.1). Upon reduction, the coordination polyhedron, best represented as a distorted trigonal bipyramid, experiences only small structural rearrangements to ensure its reversibility and rapid electron transfer.[14] Lower reduction potentials were observed for homologous green and red copper proteins with thiolates of cysteine and homocysteine substituted for methionine, respectively, since a stronger axial Cu-S bond with thiolates favours a tetragonal geometry around copper and hence stabilises the cupric state.[15]

Inspired by unusually intense absorption bands around 600 nm in blue copper proteins, a series of macrocyclic complexes containing sulphur donors was devised in the late 1970s. These complexes featured a reversible redox behaviour with very high reduction potentials, which correlate with the number of sulphur atoms, as well as chelate and macrocyclic ring sizes.[16] However, the higher reduction potential comes at a cost of compromised stability of the Cu(II) complex, whilst the stability of Cu(I) species was shown to vary little with the general ligand morphology.[17] Therefore, an optimal interplay between the biologically relevant stability constant of the Cu(II) complex and its redox potential should be attained through judicious design of the ligand. For instance, by introducing sulphur donors in thiaaza macrocycles, a fine tuning of the redox potential can easily be achieved.

Although the previous attempt to utilise 12/13/14-membered dithiadiaza macrocycles **NEC-SE/P/B** (Fig.2) as ^{64}Cu chelators proved unsuccessful, presumably due to a high lability of the Cu(II) complexes,[18] alternative ligands that form kinetically inert copper(I/II) complexes can potentially deliver a better *in vivo* performance. A previously reported dithiadiaza macrocycle **[14]aneNSNS**[19] – a dithiadiaza analogue of cyclam – and its recently reported derivative **[14]aneNSNS2POH**[20] bearing phosphonate-derivatised arms have a reasonably high redox potential to enable their facile reduction in the body ($E_{1/2}$ = 209 mV vs N.H.E. for **[14]aneNSNS**), whilst maintaining a sufficient thermodynamic stability ($LogK_{Cu}(II)_L$ = 15.15). By introducing two N-acetate pendant arms, a potentially six-coordinate ligand **NSNS2A** is obtained, which is expected to lock a highly flexible NSNS core and form a kinetically inert **Cu$^{(II)}$(NSNS2A)** complex suitable for PET imaging. The proposed ligand is reminiscent of a cyclam-derived **TE2A**,[21] which forms highly kinetically inert copper (II) complexes and was successfully tested as ^{64}Cu chelator in preclinical studies.[22]

In the present paper, we report on the synthesis and structural elucidation of Cu(I) and Cu(II) complexes with **NSNS2A** ligand by means of X-ray crystallography, EPR and NMR spectroscopies augmented by DFT and TDDFT calculations. The chelator was also radiolabelled with ^{64}Cu and injected into Wistar rats to evaluate its biodistribution and pharmacokinetics.

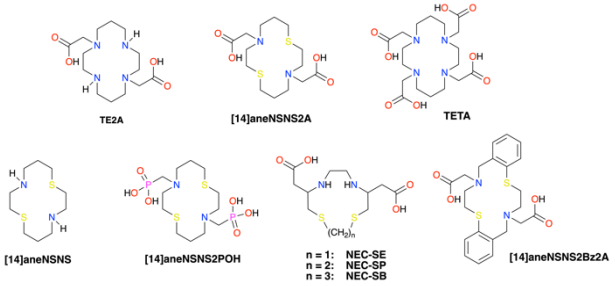

Figure 2. Structures of ligands discussed in the paper.

Results and discussion

Dithiadiaza macrocycle [14]aneNSNS was synthesised according to a previously reported procedure.[23] It was alkylated to yield an ethyl protected chelator **1** , which was hydrolysed to give **2** as an HCl double salt (Scheme 2). Cupric complex **Cu$^{(II)}$(NSNS2A)** was synthesized by stirring copper (II) acetate with **2** in water at room temperature for 10 min.

Since radiolabelling of chelators is often carried out in the presence of various buffers, such as acetate and citrate salts, their potential effect on the formation of **Cu$^{(II)}$(NSNS2A)** was also investigated. It turned out that the acetate buffer (40 mM, pH = 5.5) did not affect the UV-vis spectrum either at room temperature or after heating at 80°C for 30 min, suggesting no direct interaction between an acetate anion of the buffer and complexed copper ion. At the same time, only minor changes were observed in the UV-vis spectrum of **Cu$^{(II)}$(NSNS2A)** in a citrate buffer (0.3 M, pH = 6.0), which did not, however, include d-d transitions, and therefore are unlikely to corroborate any significant changes in the coordination environment of copper ion (Fig.S22 in ESI).

Cuprous complex **[Cu$^{(I)}$(H$_2$NSNS2A)]PF$_6$** was synthesized by reacting $Cu(MeCN)_4PF_6$ with **2** under anaerobic conditions. Formation of both complexes was verified by ^{1}H and ^{13}C NMR spectroscopy in deuterated DMSO-d_6.

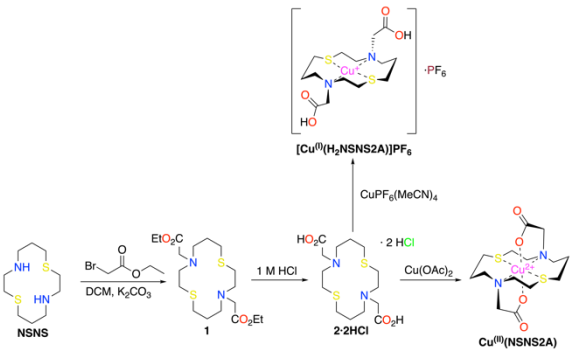

Scheme 1. Synthetic pathways for copper complexes discussed in the paper. Crystal structures of **1** and **2·2HCl** can be found in ESI.

Although attempts to obtain single crystals of copper complexes suitable for X-ray analysis proved unsuccessful, slow evaporation of the solvent from the solution containing **(1)** and $Cu(ClO_4)_2$ yielded single crystals of **[Cu(1)](ClO$_4$)$_2$** (Fig.3, Table

1). The obtained crystal structure revealed a trigonally distorted octahedral coordination of Cu^{2+} ion, with an almost perfect $[N_2S_2]$ plane (Cu-N(1) 2.074(3)Å, Cu-S(1) 2.3186(8)Å) and a straight O-Cu-O bond (Cu-O(1) 2.3256(18)) tilted in $[N_2O_2]$ plane (angle O(1)-Cu-N(1) 79.22(9)°). In a previously reported crystal structure of **[Cu(NSNS)](ClO$_4$)$_2$** with a coordination polyhedron that is best described as an axially elongated octahedron with perpendicular rhombic distortion, slightly shorter bond lengths in equatorial $[N_2S_2]$ plane were revealed (Cu-N(1) 2.0146(13)Å, Cu-S(1) 2.2954(10)Å), due to much weaker Cu-O bonding (Cu-O 2.576(2)Å). However, a similar, albeit a much smaller tilt of a perfectly straight O-Cu-O bond was still observed, this time in $[N_2O_2]$ plane (angle O-Cu-S 83.59(6)°).

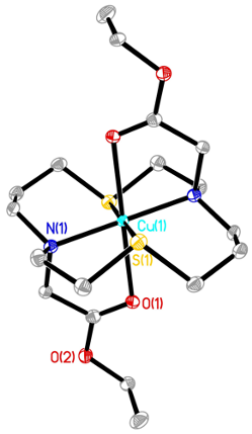

Figure 3. The thermal ellipsoid diagram showing the structure of the cationic unit for **[Cu(1)](ClO$_4$)$_2$**. Hydrogen atoms and counteranions are omitted for clarity. Thermal ellipsoids are set at 35% probability.

In a first approximation, solid state structures of metal complexes are usually assumed to be close to the solutes, as most analytical tools at our disposal can only provide indirect evidences towards a particular structure in solution. Given these circumstances, *ab initio* quantum chemical calculations can serve as a good starting point to validate and, if necessary, optimize the structure based on spectroscopic experiments. The crystal structure of **([Cu(1)](ClO$_4$)$_2$)** was used as an initial input to calculate the molecular structure of **Cu$^{(II)}$(NSNS2A)** in aqueous solution at the D3-B3LYP/def2-TZVP level of theory. In the calculated structure, the **[14]aneNSNS** macrocycle experienced notable conformational changes, with significantly elongated Cu-S bonds (Table 1), partially releasing the strain caused by the rearrangement of the macrocycle upon complexation.

This, in turn, gave rise to a remarkable elongation of Cu-S bonds (2.746Å), while leaving Cu-N bonds almost intact (2.066Å). At the same time, Cu-O bond with anionic pendant arms significantly strengthened, becoming much shorter than the bond in an analogous **Cu(TE2A)** complex (1.997Å vs 2.263Å).[21] The straight O-Cu-O bond is tilted with respect to the N_2O_2 plane by 84.27°.

The infrared spectrum in water is in line with the proposed structure, featuring symmetric and asymmetric stretching bands at frequencies typical for coordinated carboxylate groups (ν_s = 1395 cm^{-1} and ν_{as} = 1592 cm^{-1}, $\Delta = \nu_{as}-\nu_s$ = 197 cm^{-1}).

The absorption spectrum of **Cu$^{(II)}$(NSNS2A)** features two absorption bands at λ = 314 nm (ε = 2445 M^{-1}cm^{-1}, pH = 5.0) and λ = 365 nm (ε = 5770 M^{-1}cm^{-1}, pH = 5.0), which were previously assigned to N(σ)→Cu^{2+}($d_{x^2-y^2}$) and S(σ)→Cu^{2+}($d_{x^2-y^2}$) ligand-to-metal charge transfer (LMCT) states, respectively, and can be used to probe the coordination environment of copper.[24] These absorption bands are very close to the LMCT transitions observed in **[Cu(NSNS)](ClO$_4$)$_2$**, suggesting the presence of a square-planar $[N_2S_2]$ coordination environment in **Cu$^{(II)}$(NSNS2A)**, although the broad asymmetric band corresponding to *d-d* transition is bathochromically shifted (λ_{d-d} = 597 nm (ε = 98 M^{-1}cm^{-1}, pH = 5.0) in **Cu$^{(II)}$(NSNS2A)** compared to **Cu$^{(II)}$(NSNS)** (λ_{d-d} = 545 nm). The latter can serve as an evidence of the stronger axial interaction, in line with the notion of oxygen atoms of acetate pendant arms being bound to copper.

Table 1. Selected bond angles and bond lengths for copper (II) complexes discussed in the paper, as calculated by XRD (**[Cu(1)](ClO$_4$)$_2$**) or DFT (**Cu$^{(II)}$(NSNS2A)** and **[Cu$^{(II)}$(H$_2$NSNS2A)]$^{2+}$**)

	[Cu(1)](ClO$_4$)$_2$	**Cu$^{(II)}$(NSNS2A)**	**[Cu$^{(II)}$(H$_2$NSNS2A)]$^{2+}$**
Bond lengths (Å)			
Cu-O	2.3256(18), 2.3256(18)	1.997, 1.997	2.462, 2.464
Cu-S	2.3186(8), 2.3186(8)	2.746, 2.746	2.366, 2.366
Cu-N	2.074(3), 2.074(3)	2.066, 2.066	2.141, 2.142
Bond angles (°)			
N-Cu-N	180.0(3)	180.0	179.9
N-Cu-S	88.82, 91.18(8)	88.1, 91.9, 88.1, 91.9	88.4, 91.6, 88.4, 91.6
S-Cu-S	180.0	180.0	180.0
O-Cu-O	180.0	180.0	180.0
O-Cu-N	100.78(9), 79.22(9), 100.78(9), 79.22(9)	95.7, 84.3, 95.7, 84.3	103.7, 76.3, 103.6, 76.3
O-Cu-S	89.85(5), 90.15(5), 89.85(5), 90.15(5)	91.7, 88.3, 81.7, 88.3	90.3, 89.7, 90.3, 89.7
C-S-C	104.81(16), 104.81(16)	105.1, 105.1	104.4, 104.4
C-N-C	105.1(3), 105.1(3)	107.3, 107.3	106.6, 106.6

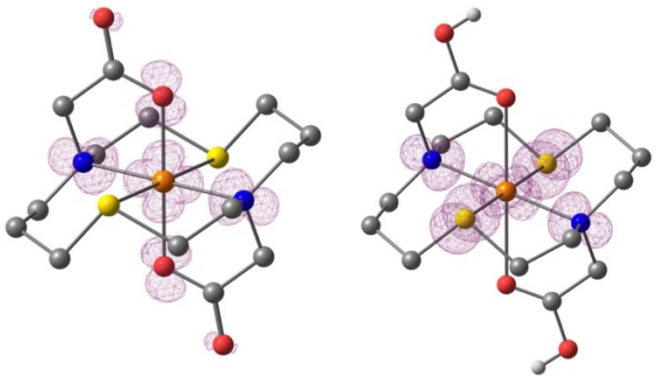

Figure 4. Spin density contour plots (contour value 0.003) of **Cu$^{(II)}$(NSNS2A)** on the left and **[Cu$^{(II)}$(H$_2$NSNS2A)]$^{2+}$** on the right based on optimised geometry from DFT calculations**.** Atoms are colour-coded as follows: Cu – orange, S – yellow, O – red, N – blue, C – dark grey, H – light grey, hydrogens attached to carbons are omitted for clarity.

At the same time, the presence of a relatively intense S(σ)→Cu^{2+}($d_{x^2-y^2}$) band contradicts to the calculated DFT structure of **Cu$^{(II)}$(NSNS2A)** (Fig.4), with the $d_{x^2-y^2}$ orbital being located in the [N_2O_2] plane and therefore providing very poor overlap, if any, with σ orbitals of the sulphur atoms. In contrast, the DFT structure of **[Cu$^{(II)}$(H$_2$NSNS2A)]$^{2+}$** with protonated acetate arms (*vide infra*) exhibits shorter Cu-S and elongated Cu-O bonds, flipping the $d_{x^2-y^2}$ orbital of Cu^{2+} into [N_2S_2] plane, consistent with the absorption spectrum in water. A similar orbital switch might be observed if acetate pendant arms of the macrocycle participate in hydrogen bonding with water molecules. Despite our efforts to obtain corresponding DFT structures with water molecules bound via hydrogen bonds, such calculations never converged. The possible role of hydrogen bonding in elongation of Cu-O bonds and rearrangement of the spin density was further elucidated by running absorption spectra in aprotic solvents, which, however, gave inconclusive results. Although the UV-vis spectrum of **Cu$^{(II)}$(NSNS2A)** in acetonitrile and 1,4-dioxane showed the expected dramatic decrease of S(σ)→Cu^{2+}($d_{x^2-y^2}$) band (in the case of acetonitrile, down to zero), the spectrum recorded in DMSO was identical to that in water (Fig.S17 in ESI). At the same time, the energy of d-d transitions experienced very little change, suggesting that no direct binding of solvent molecules to the copper ion has occurred. These experimental findings, including the assignment of transition bands, were supported by TDDFT calculations, predicting a disappearance of the S(σ)→Cu^{2+}($d_{x^2-y^2}$) transition in the spectrum of **Cu$^{(II)}$(NSNS2A)** when no protonation or other perturbation of acetate arms takes place (Fig.5). A similar phenomenon was previously reported by Archibald for two structural isomers of **Cu(TETA)** with different tetragonal elongations – one along O-Cu-O direction (crystallised from water) and one along N-Cu-N direction (crystallised from acetonitrile), across the macrocycle.[25] It was also hypothesised that hydrogen bonding might be the driving force behind the presence of the conformation with an unusual macrocyclic Jahn-Teller distortion, which possibly reflects the dynamic interchange between different conformations of the complex in solution, eventually leading to poor *in vivo* stability of **Cu(TETA)**.

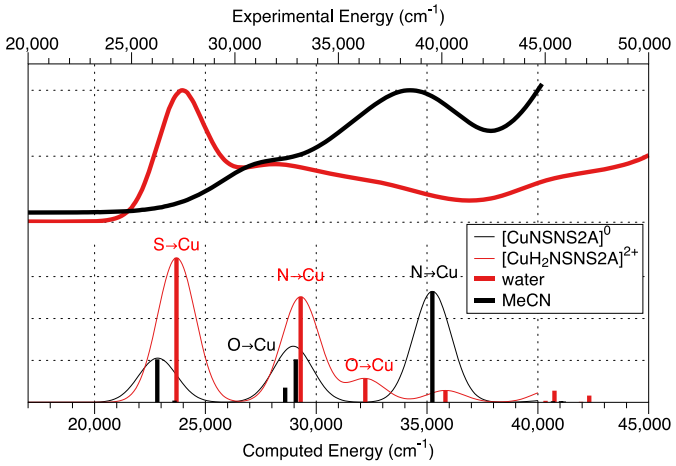

Figure 5. Experimentally observed UV-vis spectra of **Cu$^{(II)}$(NSNS2A)** in water and acetonitrile (top) and corresponding calculated spectra for **Cu$^{(II)}$(NSNS2A)** and **[Cu$^{(II)}$(H$_2$NSNS2A)]$^{2+}$** (bottom). The calculated spectra were shifted to match the corresponding experimental spectra.

The EPR spectra are characterized by slightly to moderately rhombic g- and A-tensors, the latter one being the tensor of the hyperfine interaction (hfi) of the copper nucleus (see Fig. 6 and Table 2). The principal axes X, Y, and Z of the tensors correspond to the similar axes defining the real *d*-orbital set of the Cu(II) ion, with the $d_{x^2-y^2}$ orbital carrying the unpaired electron. At least three out of four EPR turning points corresponding to (g_z, A_z) are readily observable at the low-field side of the spectra for **Cu$^{(II)}$(NSNS2A)**.

The square-planar geometry observed in a solid state can often experience distortions in solution. It has been shown that the g_z/A_z ratio can serve as a qualitative measure of the tetrahedral distortion in square-planar copper complexes. If A_z is expressed in cm^{-1} (1 cm^{-1} ≈ 30 GHz), then g_z/A_z < 130 cm correspond to the planar geometry, the values between 130 – 150 cm indicate a small to moderate departure from planarity, and still larger values (even as high as 250) result from a considerable distortion.[24, 26-28] As an example, g_z/A_z = 122 cm observed for **Cu$^{(II)}$(NSNS)**) corresponds to a planar geometry.[19] For the complex **Cu$^{(II)}$(NSNS2A)** studied in this work, the g_z/A_z ratio of 130 cm suggests that the tetrahedral distortion of the [N_2S_2] plane is relatively insignificant. Indeed, the DFT calculations show that both protonated and deprotonated complexes do not have any tetrahedral distortion.

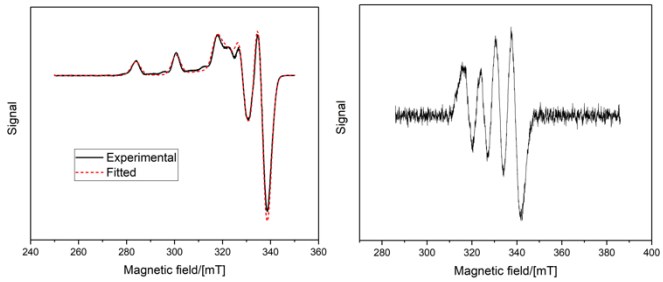

Figure 6. CW X-band EPR spectrum at 77K (solid line) with a fitted curve (dashed lines) for **Cu$^{(II)}$(NSNS2A)** (left). 45% glycerol/55% 0.1 HEPES solution (pH = 7.0). CW X-band EPR spectrum at 298K for **Cu$^{(II)}$(NSNS2A)** in water (right).

Table 2. Principal g-values and copper hyperfine couplings, A, obtained from EPR spectral fitting and calculated with DFT (*calc.*).

Complex	g_z	g_y	g_x	A_z (MHz)	A_y (MHz)	A_x (MHz)
Cu$^{(II)}$(NSNS2A) (pH = 7.0)	2.182	2.063	2.036	-504	-76	-13
Cu$^{(II)}$(NSNS2A) *calc.*	2.162	2.058	2.039	-557	30	-17
Cu$^{(II)}$(H_2NSNS2A) *calc.*	2.120	2.041	2.035	-508	-42	-39

A large body of evidence suggests that the coordination geometry of copper complexes strongly correlates with their redox behaviour. Indeed, it has been shown that a substitution of sulphur atoms for nitrogen atoms resulted in a significant increase of redox potentials.[29] Since Cu(I) species predominantly form tetrahedral complexes, a tetrahedral distortion of Cu(II) complexes would likely facilitate redox processes. For **Cu$^{(II)}$(NSNS2A)**, a quasi-reversible redox behaviour was observed ($E_{1/2}$=146 mV vs Ag/AgCl electrode, respectively, Fig.7, pH = 7.0). This value is much higher than the one previously reported for **Cu$^{(II)}$(TE2A)** ($E_{1/2}$= -1.10 V vs Ag/AgCl electrode).[22]

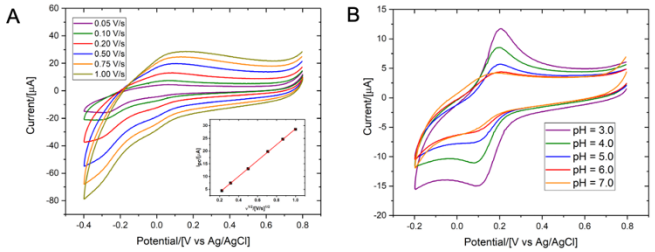

Figure 7. Cyclic voltammograms of copper complexes **Cu(NSNS2A)** upon variation of scanning rate (A, 0.1M HEPES, 0.5M KNO_3, pH = 7.0) and pH (B, 0.1M HEPES, 0.5M KNO_3). The inset in Fig.7A shows a linear dependence between the anodic peak current and the square root of scan rates.

A quasi-reversible redox behaviour was previously reported for **[Cu(NSNS)]$^{2+}$** complex in an aqueous solution with a significantly lower half wave potential ($E_{1/2}$ =-230mV or $E_{1/2}$ =-260mV vs Ag/AgCl) and a larger peak-to-peak separation (ΔE_p) that might be indicative of larger structural rearrangements upon reduction/oxidation in the absence of pendant arms.[19] At the same time, alkylation of secondary amines was shown to increase the redox potential of copper complexes, supposedly by destabilising the Cu(II) species as a result of lower donor capacity of tertiary amines.[26] On the other hand, the stability of the Cu(II) species can be potentially increased, for instance, by introducing pendant arms, which is expected to lead to a significant decrease of a redox potential. In the case of **Cu(NSNS2POH)** complex bearing two phosphonate arms, a decreased half wave potential ($E_{1/2}$ =-310 mV vs Ag/AgCl) was reported.[20] Therefore, the much higher $E_{1/2}$ values observed for **Cu$^{(II)}$(NSNS2A)** might be indicative of either lower thermodynamic stability of the Cu(II) complex, or higher stability of the Cu(I) species, although the latter was previously shown to have a much smaller impact.[17] However, a high stability constant of the complex does not necessarily translate into a higher stability *in vivo*, as, for example, has been shown for **^{64}Cu(TETA)**.[30] Instead, transchelation challenge experiments are often performed that can remotely mimic conditions experienced by the tracer in vivo, in the presence of various endogenous chelators. In the present case, a 1-hour incubation of **Cu$^{(II)}$(NSNS2A)** with 1 eq. of EDTA (0.1M MES, pH = 5.5, Fig.9) serving as a metal scavenger resulted in almost complete transchelation with the loss of the LMCT band in the UV spectrum. On the other hand, analogous tetraaza macrocycles show no metal loss under the same conditions. By following the Benesi-Hildebrand approach,[31] a conditional dissociation constant for **Cu$^{(II)}$(NSNS2A)** was estimated (K_D = 2.1(±0.34)x10^{-6} M, pH = 5.0, T = 298K, Fig.8), which is higher than the values

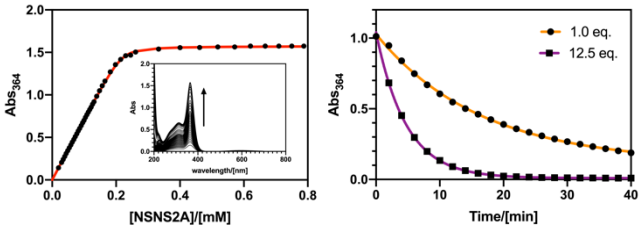

reported for **Cu$^{(II)}$(NSNS)** and related unsubstituted thiaaza macrocycles.[19]

Figure 8. A least-square fit of the binding curve for **Cu$^{(II)}$(NSNS2A)** (42 μM ClO_4^-, 0.2 mM Cu^{2+}, pH = 5.0, left) and dissociation curves for **Cu$^{(II)}$(NSNS2A)** in the presence of 1.0 and 12.5 equivalents of EDTA (0.1M MES, pH = 5.5, right).

To determine the thermodynamic stability constant, protonation constants of the ligand were estimated by ^{1}H NMR pH titration experiments (Fig.S23 and Fig.S24). Chemical shifts of macrocyclic protons were plotted as a function of pH, revealing an average logK_{H1} = 7.7 for both tertiary amines, whilst logK_{H2} = 2.5 was calculated for pendant acetate arms by monitoring a change in a chemical shift of methylene protons. Unfortunately, the resolution of our titration experiment did not allow to distinguish between the first and the second protonation constants, and therefore the obtained values were treated as the average protonation constants for both tertiary amines and both acetate arms. The obtained value $K_{Cu^{(II)}L}$ = 1.2 x10^{11} M^{-1} for **Cu$^{(II)}$(NSNS2A)** was used to calculate the stability constant $K_{Cu^{(I)}L}$ for **Cu$^{(I)}$(NSNS2A)**, using the following equation:

$$E_f = E^0_{aq} - 0.059 \log \frac{K_{Cu^{(II)}L}}{K_{Cu^{(I)}L}},$$

where E_f is a redox potential of the complex vs SHE and E^0_{aq} is the concentration potential of the aquated Cu(II/I) redox couple, for which a value of 0.13 V was utilised.[17] The resultant stability constant $\log K_{Cu^{(I)}L}$ = 14.7 is very similar to the values previously reported by Rorabacher for closely related unsubstituted thiaaza macrocyclic systems, where the average value $\log K_{Cu^{(I)}L}$ = 13.8 was reported.[17] This value was shown to vary little with the ligand morphology, regardless of the ring size, as well as the type and number of donor atoms. This correlation now seems to hold true also for complexes with N-substituted ligands, however additional examples should be studied in order to support this conclusion.

Cu$^{(II)}$(NSNS2A) complex can be reduced in aqueous solutions by sodium dithionate, although a complete reduction was not observed even in the presence of a large excess of the reductant (Fig.S15 in ESI).

The diamagnetic complex [**Cu$^{(I)}$(H$_2$NSNS2A)**]$^+$ was characterized by ^{1}H and ^{13}C NMR spectroscopy. The presence of five broadened multiplets corresponding to the [14]-aneNSNS macrocycle backbone indicates the retention of its time-averaged symmetry (C_2) upon complexation. NMR spectra of [**Cu$^{(I)}$(H$_2$NSNS2A)**]$^+$ showed no changes when heated up to 65°C, as shown in Fig.S2 (ESI).

The observed C_2 symmetry for DMSO-d$_6$ solutions of the complex can either suggest the presence of two tetrahedral species which are in fast exchange resulting in an averaged octahedral conformation or the presence of genuine square-planar [NSNS] coordination around Cu(I) ion. Although the presence of broadened peaks in ^{1}H NMR spectra, whose width is insensitive to temperature variation within studied range, makes the former proposition unlikely, the latter seems also hardly plausible due to the paucity of such precedents in the literature.[32-35] Indeed, the examples of square-planar Cu(I) complexes are extremely scarce, as diamagnetic Cu(I) favours tetrahedral coordination. However a distorted square-planar coordination was previously reported for another 14-membered macrocycle in a solid state.[32, 36] Surprisingly, DFT calculation performed for [**Cu$^{(I)}$(H$_2$NSNS2A)**]$^+$ revealed a perfect square-planar coordination of Cu(I) (Fig.9), featuring long Cu-N bonds (2.403 Å). On the other hand, the deprotonated species **Cu$^{(I)}$(NSNS2A**), which might be observed at higher pH exhibits a typical tetrahedral coordination with Cu(I) bound to two nitrogen atoms and one sulphur atoms of the macrocycle, as well as to the oxygen atom of the pendant acetate arm (Fig.9).

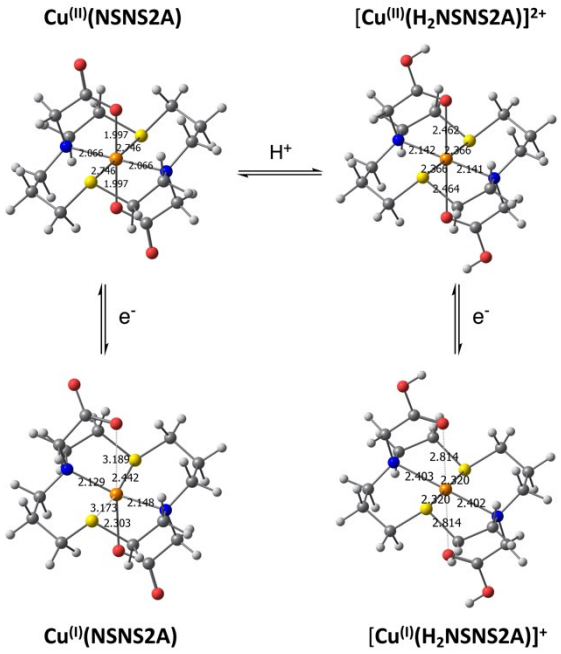

Figure 9. Optimised structures of **Cu$^{(I/II)}$(NSNS2A)$^{-/0}$** and its protonated version **[Cu$^{(I/II)}$(H$_2$NSNS2A)]$^{+/2+}$**. Geometry was optimized using D3-B3LYP/def2-TZVP in a continuum model of water (SMD parametrization).

Although the retention of square-planar coordination for both Cu(I) and Cu(II) species in solution might have far-reaching implications, including unusual photophysical performance involving strongly red-shifted metal-to-ligand charge transfer (MLCT) state and elevated redox potential, one should treat these initial findings very cautiously. However, even if square-planar coordination of [**Cu$^{(I)}$(H$_2$NSNS2A)**]$^+$ in DMSO solution in the absence of competing anions can be proved by other techniques, such as EXAFS, this is unlikely to be the case for biologically relevant aqueous systems with multiple competing anions that can bind to the Cu(I) ion, especially at elevated pH values, when deprotonated **Cu$^{(I)}$(NSNS2A)** is predicted to adopt a tetrahedral coordination environment. Our attempts to detect any unusually red-shifted absorption bands for cuprous species were futile and require closer inspection in future studies.

Variation of pH within the range of 3-7 revealed a sharpening of reduction/oxidation peaks for **Cu$^{(II)}$(NSNS2A)** as the pH decreased that was initially attributed to the protonation of the acetate arms. The presence of only subtle changes in the EPR and UV spectra at different pH (Table 2; Fig.S16 and Fig.S21 in ESI) rules out any significant structural transformations around the copper ion upon anticipated protonation of acetate arms, in accord with the previously reported copper (II) complex with **[14]-ane-[NSNS2Bz2A]**.[37] In the present case, in the calculated structure of **[Cu$^{(II)}$(H$_2$NSNS2A)]$^{2+}$** with protonated acetate arms, the copper ion retains a square-planar [N$_2$S$_2$] coordination (Fig.9), whereas protonation weakens Cu-O bonds, leading to an elongation of the octahedron. This results in a significant shortening of Cu-S bonds and elongation of Cu-N bonds. Such pronounced changes should have clearly resulted in a more noticeable changes in the EPR spectra, as well as in UV spectra

and cyclic voltammetry, suggesting that the protonation of acetate arms at pH above 3 is unlikely. No LMCT bands were detected in the UV-vis spectrum at pH below 2.5, suggesting full dissociation of the complex upon protonation of the acetate arms or tertiary nitrogen atoms of the macrocycle. On a closer inspection, a formation of a precipitate was observed at pH just slightly above 7.0, suggesting that the observed broadening of reduction/oxidation peaks might be a result of partial aggregation at higher pH.

Radiolabelled Cu-64 complex, **^{64}Cu$^{(II)}$(NSNS2A)**, was synthesized by mixing $^{64}CuCl_2$ with the ligand dissolved in 0.3M ammonium citrate buffer (pH = 6.0) and heating the reaction mixture at 80°C for 10 min. The progress of the radiolabelling was monitored by radio-HPLC using a HILIC column (Fig.S18 in ESI). As a control probe, a tetraaza analogue, **^{64}Cu(TE2A)**, was selected, which was previously evaluated in preclinical studies.[22, 38]

Each radiotracer was injected in three Wistar rats, who were dynamically scanned for 60 min using a 4.7T PET/MRI scanner and then euthanized 90 min post injection (Fig.10). Eleven different tissue specimens were harvested post-mortem and their radioactivity was counted. The half-life in blood was fitted with a biexponential decay curve ($t_{1/2}$ = 1.2 min/9.4 min for **^{64}Cu$^{(II)}$(NSNS2A)** and 0.7 min/11.8 min for **^{64}Cu(TE2A)**). Rapid clearance from blood was followed by a renal filtration as well as an uptake into the liver for **^{64}Cu$^{(II)}$(NSNS2A),** whereas **^{64}Cu(TE2A)** was predominantly filtered by the kidneys. The latter finding is in line with a previously reported study and is typical for other renally excreted tetraaza macrocyclic copper-64 complexes.[22] As well as renal filtration, there also appeared to be some uptake into the renal cortex in the case of **^{64}Cu$^{(II)}$(NSNS2A),** as the kidney signal did not decline at later time points.

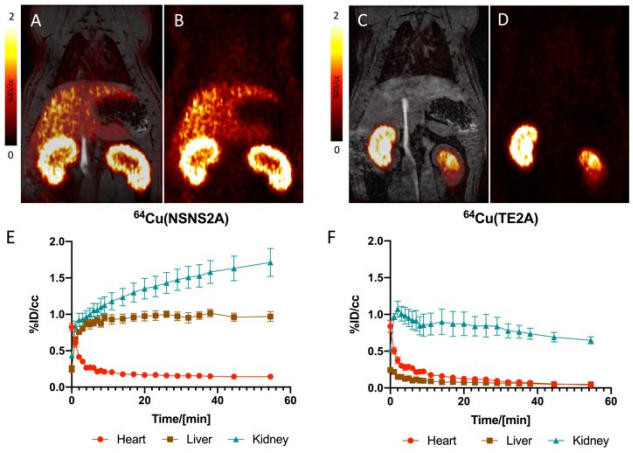

Figure 10. Coronal PET/MR (A) and PET (B) images of a rat injected with **^{64}Cu$^{(II)}$(NSNS2A)** 30 min post injection and a corresponding time-activity curve (E). Coronal PET/MR (C) and PET (D) images of a rat injected with **^{64}Cu(TE2A)** 30 min post injection and a corresponding time-activity curves for blood, liver, and kidneys (F).

For **^{64}Cu$^{(II)}$(NSNS2A)**, the PET signal from the liver plateaued at ca. 8 min post injection and remained unchanged for the rest of the scan. The absence of clearance from the liver suggests a transchelation/dissociation of the ^{64}Cu(II) and binding to liver proteins in hepatocytes and a long-term retention. Some evidence of hepatobiliary elimination is also observed by the appearance of the signal in the intestines with time. By comparing the residual radioactivity (in %ID/g) in various organs at 90 minutes post injection (Fig.11), a much lower tracer uptake in all tissues was observed for **^{64}Cu(TE2A)** than for **^{64}Cu$^{(II)}$(NSNS2A**). In fact, for **^{64}Cu(TE2A)**, a very low uptake in the liver detected 90 min post injection (0.12 %ID/g) is in agreement with the previously reported value (0.073 %ID/g 24h post injection), consistent with a very high *in vitro* stability of the complex.[22] On the other hand, a remarkably higher liver uptake for **^{64}Cu$^{(II)}$(NSNS2A)** (2.15 %ID/g) is comparable with the reported the values for similar dithiadiaza macrocyclic complexes **^{64}Cu(NEC-SE/SP/SB)** reported by Lewis and Anderson (ca. 3 %ID/g).[18] Similar numbers were reported for copper-67 chloride in rats,[39] reflecting a low *in vivo* stability of these tracers with an apparent metal loss occurring shortly after injection.

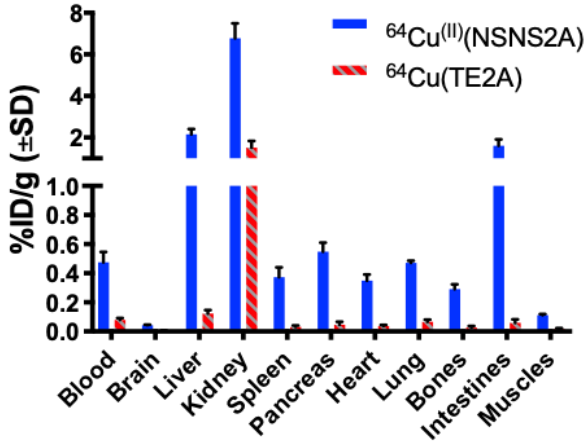

Figure 11. Biodistribution data (%ID/g) for **^{64}Cu$^{(II)}$(NSNS2A)** (N=3) and **^{64}Cu(TE2A)** (N=3) at 90 min post injection.

Conclusions

Copper (I)/(II) complexes with a new dithiadiaza macrocyclic ligand **NSNS2A** were reported and their structures in solution were thoroughly investigated by a combination of spectroscopic techniques and DFT calculations. The latter predicted the change in the orientation of tetragonal distortion in **Cu$^{(II)}$(NSNS2A**) upon protonation and possibly hydrogen bonding of pendant acetate arms, supposedly leading to a relatively high lability of the complex in aqueous media. A very unusual square-planar coordination of copper (I) ion was proposed for the cuprous complex **[Cu$^{(I)}$(H$_2$NSNS2A)]$^+$** which, however, requires further validation in future studies. *In vivo* study performed with a radiolabelled compound **^{64}Cu$^{(II)}$(NSNS2A**) revealed a suboptimal stability that is much lower than exhibited by its tetraaza analogue, in line with *in vitro* experiments. Given these results along with the findings previously reported for a similar [N_2S_2] system,[18] we can conclude that the stability of copper complexes with sulphur-containing macrocycles appears to be insufficient for their successful use in PET imaging.

Experimental section

^{1}H and ^{13}C NMR spectra were recorded on Varian 400 MHz and JEOL 500 MHz systems. FTIR spectra were collected on a Jasco 4600 spectrophotometer running Spectra Manager CFR®, where samples were prepared as a neat oil or solid on a ZnSe window using attenuated total reflectance (ATR). Melting points were obtained on a MeltTemp melting point apparatus and are uncorrected. High-resolution mass spectra (HRMS) were recorded on a time-of-flight JEOL JMST1000LC spectrometer with a DART ion source. Liquid chromatography-mass spectrometry (LC-MS) was performed using an Agilent 1200 Series HPLC interfaced to an Agilent 6130 single quadrupole electrospray mass spectrometer and to a Daly conversion dynode detector with UV detection at 220, 254, and 280 nm. UV-vis spectra were recorded on a SpectraMax M2 spectrophotometer using quartz cuvettes with a 1 cm path length. Cyclic voltammetry measurements were performed using a Nuvant EZstat Pro potentiostat equipped with Ag/Ag^{+} (3 M NaCl) reference electrode, Pt wire counter electrode, and glassy carbon working electrode. Measurements were performed at room temperature in 0.5 M KNO_3 electrolyte. The ferri/ferrocyanide couple was used as an internal standard. The radiochemical purity of the dose to be injected was determined by radio-HPLC (Agilent 1100 Series HPLC unit with a Carroll/Ramsey radiation detector with a silicon PIN photodiode) and radio-TLC (Bioscan AR-2000).

EPR spectroscopy

The EPR experiments were carried out at the University of Arizona EPR Facility, on the X-band EPR spectrometer Elexsys E500 (Bruker Biospin) equipped with the rectangular resonator operating in TE_{102} mode. In the measurements performed at 77 K and room temperature (~298 K), the microwave frequencies were 9.44 GHz and 9.65 GHz, respectively. The microwave power was 2 mW, and the magnetic field modulation amplitude was 0.5 mT. EPR spectra were fitted using EasySpin software.

Binding studies

Solution 1: 0.2 mM solution of $Cu(ClO_4)_2$ was prepared by dissolving $Cu(ClO_4)_2$ in milli-Q water (pH = 5.0, adjusted with 60% $HClO_4$). Solution 2: 2.0 mM solution of NSNS2A was prepared by dissolving 2·2HCl in solution 1. Solution 2 was added incrementally to solution 1 in a quartz cuvette and the UV-vis spectrum was recorded after every addition. Absorption at λ = 364 nm was plotted as a function of NSNS2A concentration and fitted in MatLab using the following equation:

$$\frac{A}{\varepsilon} = 0.5 * ([Cu_T] + [NSNS2A_T] + K_D - \sqrt{([Cu_T] + [NSNS2A_T] + K_D)^2 - 4 * [Cu_T] * [NSNS2A_T]}),$$

where A is the absorbance, ε is the molar attenuation coefficient, $[Cu_T]$ is the total concentration of copper, $[NSNS2A_T]$ is the total concentration of NSNS2A chelator and K_D is the dissociation constant, which is being determined.

Stability tests

$Cu^{(II)}$(NSNS2A) was dissolved in a MES buffer (0.1M, pH = 5.5), and the absorption spectrum was recorded in a quartz cuvette. EDTA was added, the solution was vigorously shaken, and the absorption spectra were recorded every two minutes until the signal at λ = 364 nm disappeared.

Radiolabelling

$^{64}CuCl_2$ was purchased from the University of Wisconsin-Madison cyclotron lab. All buffers and solutions were prepared using ultrapure water and were chelex-treated for 24h before use. $^{64}CuCl_2$ (28 mCi) was diluted with 1 mL of citrate buffer (0.3M, pH = 6.0) and an aliquot (50 µL) was added to the ligand. The latter was prepared by mixing 0.3 mL of 1.8 mM NSNS2A in water with 0.2 mL citrate buffer (0.3M, pH = 6.0). The reaction mixture was heated at 80°C for 10 min. The solution was cooled down and was filtered through a sterile syringe filter. The formation of $^{64}Cu^{(II)}$(NSNS2A) was confirmed by radio-HPLC. A similar protocol was used for radiolabelling of ^{64}Cu(TE2A), except a higher concentration (25 mM) of the ligand solution was used. The formation of ^{64}Cu(TE2A) was confirmed by radio-TLC, as previously reported.[22] Both tracers were diluted with PBS and sterile filtered prior to injection.

Imaging and biodistribution

All experiments and procedures were performed in accordance with the National Institutes of Health's "Guide for the Care and Use of Laboratory Animals" and were approved by the Massachusetts General Hospital Institutional Animal Care and Use Committee. 7 Wistar rats (male, 378g-456g) were obtained from Charles River Labs (Wilmington, MA). They were anesthetised with 2% of isoflurane in oxygen and the tracer (120-200 µCi) was administered by IV injection. Quantifications of ^{64}Cu activity in each injected dose was determined using a Capintec CRC-15PET dose calibrator. Rats were imaged on a 4.7 Tesla PET/MRI scanner (Bruker, Billerica MA) and a Bruker PET insert, placed in a holder and heated with warm air. The respiration rate was monitored all through the experiment using Small Animal Instruments (SA Inc.) monitoring equipment and software. MR imaging protocol included 2 T_1-weighted 3D FLASH (Fast Low Angle Shot) sequences, covering most of the body, with the following parameters: echo time (TE) = 3.1 ms, repetition time (TR) = 17 ms, field of view (FOV) = 85 x 64 x 40 mm, imaging resolution = 0.221 x 0.327 x 0.625 mm^3/voxel, respiratory triggering, and a flip angle = 15 degrees in the first sequence and 30 degrees in the second. All other parameters were identical. A 3D T_2-weighted TurboRARE 3 sequence was also acquired with parameters: TE = 2.8 ms, TR = 500 ms, FPV = 80 x 60 x 40 mm, resolution = 0.208 x 0.313 x 0.833 mm^3/voxel, RARE factor = 8, and respiratory triggering. To measure PET signal, Amide software was used to draw ROIs on MR images, which were co-registered with the PET images. 3D FLASH images were used for drawing ROIs. Right kidney ROIs were

drawn freehand to cover one entire kidney. For the liver and the heart, ellipsoids were placed centered in the liver and the left chamber of the heart, respectively. Time-activity data were acquired from these ROIs. As the data itself was decay corrected during reconstruction, no decay correction was applied to the ROI data. Rats were sacrificed 90 min post injection and the following organs and tissues were collected and weighed: brain, kidneys, liver, heart, spleen, pancreas, urine, blood, lungs, femur, intestines and leg muscle. The counts in each organ were measured using a gamma counter (Wizard, Perkin Elmer) and decay corrected.

Synthesis

TE2A was synthesised as previously reported.[22]

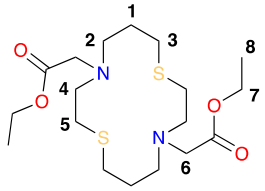

Diethyl 2,2'-(1,8-dithia-4,11-diazacyclotetradecane-4,11-diyl)diacetate (1). A 25 mL round bottom flask equipped with a septum and magnetic stir bar was charged with 1,8-dithia-4,11-diazacyclotetradecane (0.100 g, 0.427 mmol), anhydrous potassium carbonate (0.295 g, 2.14 mmol), dichloromethane (4.3 mL) and bromo ethyl acetate (0.1 mL, 0.901 mmol) in the indicated order. The reaction was stirred at room temperature for 12 h and filtered through a pad of celite. The light yellow solution was concentrated in vacuo, recrystallized in minimal amounts of ethanol and filtered affording diethyl 2,2'-(1,8-dithia-4,11-diazacyclotetradecane-4,11-diyl)diacetate (0.134 g, 0.329 mmol) in a 77% yield as a white crystalline solid. MP = 103-105 °C. ^{1}H NMR (400 MHz, $CDCl_3$) δ 4.15 (H^7, q, *J* = 7.1 Hz, 4H), 3.36 (H^6, s, 4H), 2.86 (H^4, t, *J* = 7.8, 6.2 Hz, 4H), 2.76 (H^2, t, *J* = 6.4 Hz, 4H), 2.66 (H^3, H^5, dt, *J* = 8.7, 7.0 Hz, 8H), 1.77 (H^1, p, *J* = 6.6 Hz, 4H), 1.26 (H^8, t, *J* = 7.1 Hz, 6H). ^{13}C NMR (101 MHz, $CDCl_3$) δ 171.13 (**C**OOEt), 60.3 (C^7), 55.3 (C^6), 52.9 (C^4), 52.5 (C^2), 29.9 (C^5), 29.2 (C^3), 27.7 (C^1), 14.3 (C^8). IR ν_{max} 2979, 2923, 2847, 1727, 1458, 1415, 1186, 1135, 1033 cm^{-1}. HRMS (ESI) *m/z* [M+Na$^+$] calcd. for $C_{18}H_{34}N_2NaS_2$ 429.1852, found 429.1854.

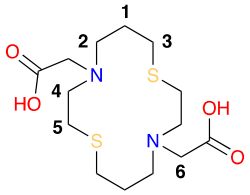

2,2'-(1,8-dithia-4,11-diazacyclotetradecane-4,11-diyl)diacetic acid dihydrochloride (2). A 5 mL round bottom flask equipped with a magnetic stir bar and septum was charged with 1 M HCl (1.2 mL) and diethyl 2,2'-(1,8-dithia-4,11-diazacyclotetradecane-4,11-diyl)diacetate (0.050 g, 0.123 mmol) and refluxed for 6 hours. The solution was concentrated in vacuo to provide 2,2'-(1,8-dithia-4,11-diazacyclotetradecane-4,11-diyl)diacetic acid dihydrochloride (0.052 g, 0.123 mmol) as a white solid in quantitative yield. ^{1}H NMR (400 MHz, D_2O) δ 4.00 (H^6, s, 4H), 3.44 (H^4, m, 4H), 3.35 (H^2, m, 4H), 2.89 (H^5, dd, *J* = 8.9, 6.8 Hz, 4H), 2.61 (H^3, t, *J* = 7.4 Hz, 4H), 1.97 (H^1, p, *J* = 7.0 Hz, 4H). ^{13}C NMR (101 MHz, D_2O) δ 168.1 (**C**OOH), 55.0 (C^6), 51.9 (C^4), 51.6 (C^2), 26.9 (C^3), 23.1 (C^5), 22.7 (C^1). IR ν_{max} 3375, 2918, 2498, 2426, 2363, 1737, 1635, 1480, 1467, 1439, 1410, 1241, 1214, 1025, 971, 923 cm^{-1}. HRMS (ESI) *m/z* [M-2HCl+H$^+$]$^+$ calcd for $C_{14}H_{27}O_4N_2S_2$ 351.1407, found 351.1407.

2,2'-(1,8-dithia-4,11-diazacyclotetradecane-4,11-diyl)diacetate copper(II) complex, Cu$^{(II)}$(NSNS2A). A 5 mL round bottom flask was equipped with a magnetic stir bar, nitrogen inlet, and rubber septum was charged with 2,2'-(1,8-dithia-4,11-diazacyclotetradecane-4,11-diyl)diacetic acid dihydrochloride salt (0.054 g, 0.128 mmol), MilliQ water (1 mL), acetonitrile (1 mL) and copper(II) acetate (0.030 g, 0.128 mmol). The dark red solution was stirred at 23 °C for 10 min and sonicated at 23 °C for 5 min. The solution was concentrated in vacuo providing a red solid in quantitative yield. HRMS (ESI) m/z [M-2H$^+$+Na$^+$]$^+$ calcd for $C_{14}H_{24}O_4N_2CuNaS_2$ 434.0366, found 434.0366.

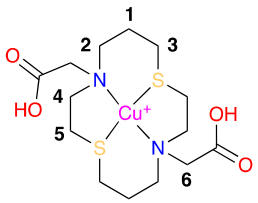

copper(I) hexafluorophosphate-2,2'-(1,8-dithia-4,11-diazacyclotetradecane-4,11-diyl)diacetic acid, Cu$^{(I)}$(H_2NSNS2A). A 5mm NMR tube, flushed with nitrogen, was charged with 2,2'-(1,8-dithia-4,11-diazacyclotetradecane-4,11-diyl)diacetic acid ·2HCl (0.020 g, 0.047 mmol) and DMSO-d_6 (1.5 mL, 0.031 M). The solution was then degassed (3x freeze-pump-thaw cycles), using Schlenk techniques, and charged with freshly prepared tetrakis(acetonitrile)copper(I) hexafluorophosphate (0.018 g, 0.047 mmol). The solution/NMR tube was warmed for 5 min at 50 °C via external water bath, then sonicated at 23 °C for 20 s. The clear solution was then subjected to NMR experiments. ^{1}H NMR (400 MHz, DMSO-d_6) δ 4.08 (H^6, s, 4H), 3.34 (H^4, m, 4H), 3.17 (H^2, m, 4H), 2.87 (H^5, m, 4H), 2.58 (H^3, m, 4H), 1.81 (H^1, m, 4H). ^{13}C NMR (101 MHz, DMSO-d_6) δ 168.2 (**C**OOH), 54.5 (C^6), 50.7 (C^4), 50.6 (C^2), 25.4 (C^3), 23.0 (C^5), 21.5 (C^1).

X-ray Crystallographic Data Collection and Structure Solution and Refinement

Crystals were obtained from the slow evaporation of a saturated solution of corresponding solvent at room temperature and stored under atmospheric conditions. Single crystal data for all structures were collected on a Bruker CCD-based diffractometer with dual Cu/Mo ImuS microfocus optics

(Cu Kα radiation, λ =1.54178 Å or Mo Kα radiation, λ = 0.71073). Crystals were mounted on a cryoloop using Paratone oil and placed under a steam of nitrogen at 100 K (Oxford Cryosystems). The data were corrected for absorption with the SADABS program. The structures were refined using Bruker SHELXTL Software Package (Version 6.1) and were solved using direct methods until the final anisotropic full-matrix least squares refinement of F2 converged.28 Electronic Supplementary Information (ESI) available: CCDC 2003358, 2003359 and 2003361 contain the supplementary crystallographic data for this paper. These data can be obtained free of charge from The Cambridge Crystallographic Data Centre via www.ccdc.cam.ac.uk/data_request/cif.

Computational details

Geometry optimisation and harmonic frequencies calculations were performed using Gaussian16 software package[40] with hybrid B3LYP functional and triple-zeta def2-TZVP basis set[41] with empirical account of dispersion interactions using D3[42] parametrisation, and SMD[43] continuum model of water. EPR parameters were calculated with ORCA 4.1[44, 45] for optimised geometries using B3LYP/def2-TZVP and core polarised CP(PPP)[46] basis set on Cu with refined grid. Spin-orbit coupling was calculated using SOMF(1X)[47] mean-field approximation. TD-DFT calculations of UV-Vis spectra were performed with ORCA 4.1 using B3LYP/def2-TZVP basis set for optimised structures.

Acknowledgements

S.S. wants to thank Dr. Mariane Le Fur for her help with radiolabelling and fruitful discussions. P.C. acknowledges support of the National Institutes of Health Office of the Director for instrumentation support (OD010650, OD023503, OD025234). C.J.Z thanks Ohio Board of Regents for funds used to purchase the Bruker-Nonius Apex CCD X-ray diffractometer.

Notes and references

‡ Footnotes relating to the main text should appear here. These might include comments relevant to but not central to the matter under discussion, limited experimental and spectral data, and crystallographic data.
§
§§
etc.

1. J. Kardos, L. Heja, A. Simon, I. Jablonkai, R. Kovacs and K. Jemnitz, *Cell Commun Signal*, 2018, **16**, 71.
2. L. A. Bass, M. Wang, M. J. Welch and C. J. Anderson, *Bioconjug Chem*, 2000, **11**, 527-532.
3. C. A. Boswell, X. Sun, W. Niu, G. R. Weisman, E. H. Wong, A. L. Rheingold and C. J. Anderson, *J Med Chem*, 2004, **47**, 1465-1474.
4. Z. Cai and C. J. Anderson, *J Labelled Comp Radiopharm*, 2014, **57**, 224-230.
5. N. A. Zia, C. Cullinane, J. K. Van Zuylekom, K. Waldeck, L. E. McInnes, G. Buncic, M. B. Haskali, P. D. Roselt, R. J. Hicks and P. S. Donnelly, *Angew Chem Int Ed Engl*, 2019, **58**, 14991-14994.
6. J. M. Kelly, S. Ponnala, A. Amor-Coarasa, N. A. Zia, A. Nikolopoulou, C. Williams, Jr., D. J. Schlyer, S. G. DiMagno, P. S. Donnelly and J. W. Babich, *Mol Pharm*, 2020, **17**, 1954-1962.
7. K. S. Woodin, K. J. Heroux, C. A. Boswell, E. H. Wong, G. R. Weisman, W. Niu, S. A. Tomellini, C. J. Anderson, L. N. Zakharov and A. L. Rheingold, *European Journal of Inorganic Chemistry*, 2005, **2005**, 4829-4833.
8. M. Le Fur, M. Beyler, N. Le Poul, L. M. Lima, Y. Le Mest, R. Delgado, C. Platas-Iglesias, V. Patinec and R. Tripier, *Dalton Trans*, 2016, **45**, 7406-7420.
9. O. C. Brown, J. Baguna Torres, K. B. Holt, P. J. Blower and M. J. Went, *Dalton Trans*, 2017, **46**, 14612-14630.
10. E. Bodio, M. Boujtita, K. Julienne, P. Le Saec, S. G. Gouin, J. Hamon, E. Renault and D. Deniaud, *ChemPlusChem*, 2014, **79**, 1284-1293.
11. Z. Xiao, P. S. Donnelly, M. Zimmermann and A. G. Wedd, *Inorg Chem*, 2008, **47**, 4338-4347.
12. P. J. Barnard, J. P. Holland, S. R. Bayly, T. J. Wadas, C. J. Anderson and J. R. Dilworth, *Inorg Chem*, 2009, **48**, 7117-7126.
13. R. H. Holm, P. Kennepohl and E. I. Solomon, *Chem Rev*, 1996, **96**, 2239-2314.
14. J. J. Warren, K. M. Lancaster, J. H. Richards and H. B. Gray, *J Inorg Biochem*, 2012, **115**, 119-126.
15. K. M. Clark, Y. Yu, N. M. Marshall, N. A. Sieracki, M. J. Nilges, N. J. Blackburn, W. A. van der Donk and Y. Lu, *J Am Chem Soc*, 2010, **132**, 10093-10101.
16. E. R. Dockal, T. E. Jones, W. F. Sokol, R. J. Engerer, D. B. Rorabacker and L. A. Ochrymowycz, *J Am Chem Soc*, 1976, **98**, 4322-4324.
17. E. A. Ambundo, M.-V. Deydier, A. J. Grall, N. Aguera-Vega, L. T. Dressel, T. H. Cooper, M. J. Heeg, L. A. Ochrymowycz and D. B. Rorabacher, *Inorganic Chemistry*, 1999, **38**, 4233-4242.
18. G. Papini, S. Alidori, J. S. Lewis, D. E. Reichert, M. Pellei, G. Gioia Lobbia, G. B. Biddlecombe, C. J. Anderson and C. Santini, *Dalton Trans*, 2009, DOI: 10.1039/b808831d, 177-184.
19. T. L. Walker, S. Mula, W. Malasi, J. T. Engle, C. J. Ziegler, A. van der Est, J. Modarelli and M. J. Taschner, *Dalton Trans*, 2015, **44**, 20200-20206.
20. I. S. Taschner, E. Aubuchon, B. R. Schrage, C. J. Ziegler and A. van der Est, *Dalton Trans*, 2020, **49**, 3545-3552.
21. J. Chapman, G. Ferguson, J. F. Gallagher, M. C. Jennings and D. Parker, *Journal of the Chemical Society, Dalton Transactions*, 1992, DOI: 10.1039/dt9920000345.
22. D. N. Pandya, J. Y. Kim, J. C. Park, H. Lee, P. B. Phapale, W. Kwak, T. H. Choi, G. J. Cheon, Y. R. Yoon and J. Yoo, *Chem Commun (Camb)*, 2010, **46**, 3517-3519.
23. T. L. Walker, W. Malasi, S. Bhide, T. Parker, D. Zhang, A. Freedman, J. M. Modarelli, J. T. Engle, C. J. Ziegler, P. Custer, W. J. Youngs and M. J. Taschner, *Tetrahedron Letters*, 2012, **53**, 6548-6551.
24. D. E. Nikles, M. J. Powers and F. L. Urbach, *Inorganic Chemistry*, 1983, **22**, 3210-3217.
25. J. D. Silversides, C. C. Allan and S. J. Archibald, *Dalton Trans*, 2007, DOI: 10.1039/b615329a, 971-978.

26. E. V. Rybak-Akimova, A. Y. Nazarenko, L. Chen, P. W. Krieger, A. M. Herrera, V. V. Tarasov and P. D. Robinson, *Inorganica Chimica Acta*, 2001, **324**, 1-15.
27. U. Sakaguchi and A. W. Addison, *Journal of the Chemical Society, Dalton Transactions*, 1979, DOI: 10.1039/dt9790000600.
28. A. W. Addison, in *Copper Coordination Chemistry: Biochemical and Inorganic Perspectives*, ed. J. Z. K.D. Karlin, Adenine Press, New York, 1983.
29. M. M. Bernardo, M. J. Heeg, R. R. Schroeder, L. A. Ochrymowycz and D. B. Rorabacher, *Inorganic Chemistry*, 1992, **31**, 191-198.
30. C. J. Anderson and R. Ferdani, *Cancer Biother Radiopharm*, 2009, **24**, 379-393.
31. H. A. Benesi and J. H. Hildebrand, *Journal of the American Chemical Society*, 1949, **71**, 2703-2707.
32. R. R. Gagne, J. L. Allison and G. C. Lisensky, *Inorganic Chemistry*, 1978, **17**, 3563-3571.
33. P. M. Cheung, R. F. Berger, L. N. Zakharov and J. D. Gilbertson, *Chem Commun (Camb)*, 2016, **52**, 4156-4159.
34. N. K. Shee, D. Das, F. A. Oluwafunmilayo Adekunle, M. G. B. Drew and D. Datta, *Inorganica Chimica Acta*, 2011, **366**, 198-202.
35. E. W. Dahl and N. K. Szymczak, *Angew Chem Int Ed Engl*, 2016, **55**, 3101-3105.
36. R. R. Gagne, J. L. Allison and D. M. Ingle, *Inorganic Chemistry*, 1979, **18**, 2767-2774.
37. D. Funkemeier and R. Mattes, *Chemische Berichte*, 1991, **124**, 1357-1362.
38. D. N. Pandya, J. Y. Kim, W. Kwak, J. C. Park, M. B. Gawande, G. I. An, E. K. Ryu and J. Yoo, *Nucl Med Mol Imaging*, 2010, **44**, 185-192.
39. C. J. Mathias, M. J. Welch, M. A. Green, H. Diril, C. F. Meares, R. J. Gropler and S. R. Bergmann, *J. Nucl. Med.*, 1991, **32**, 475-480.
40. M. J. Frisch, G. W. Trucks, H. B. Schlegel, G. E. Scuseria, M. A. Robb, J. R. Cheeseman, G. Scalmani, V. Barone, G. A. Petersson, H. Nakatsuji, X. Li, M. Caricato, A. V. Marenich, J. Bloino, B. G. Janesko, R. Gomperts, B. Mennucci, H. P. Hratchian, J. V. Ortiz, A. F. Izmaylov, J. L. Sonnenberg, Williams, F. Ding, F. Lipparini, F. Egidi, J. Goings, B. Peng, A. Petrone, T. Henderson, D. Ranasinghe, V. G. Zakrzewski, J. Gao, N. Rega, G. Zheng, W. Liang, M. Hada, M. Ehara, K. Toyota, R. Fukuda, J. Hasegawa, M. Ishida, T. Nakajima, Y. Honda, O. Kitao, H. Nakai, T. Vreven, K. Throssell, J. A. Montgomery Jr., J. E. Peralta, F. Ogliaro, M. J. Bearpark, J. J. Heyd, E. N. Brothers, K. N. Kudin, V. N. Staroverov, T. A. Keith, R. Kobayashi, J. Normand, K. Raghavachari, A. P. Rendell, J. C. Burant, S. S. Iyengar, J. Tomasi, M. Cossi, J. M. Millam, M. Klene, C. Adamo, R. Cammi, J. W. Ochterski, R. L. Martin, K. Morokuma, O. Farkas, J. B. Foresman and D. J. Fox, *Journal*, 2016.
41. F. Weigend and R. Ahlrichs, *Physical Chemistry Chemical Physics*, 2005, **7**, 3297-3305.
42. S. Grimme, J. Antony, S. Ehrlich and H. Krieg, *The Journal of Chemical Physics*, 2010, **132**, 154104.
43. A. V. Marenich, C. J. Cramer and D. G. Truhlar, *The Journal of Physical Chemistry B*, 2009, **113**, 6378-6396.
44. F. Neese, *WIREs Computational Molecular Science*, 2012, **2**, 73-78.
45. F. Neese, *WIREs Computational Molecular Science*, 2018, **8**, e1327.
46. F. Neese, *Inorganica Chimica Acta*, 2002, **337**, 181-192.
47. F. Neese, *The Journal of Chemical Physics*, 2005, **122**, 034107.